Velocities and Flux of the Filchner Ice Shelf and its Tributaries determined from Speckle Tracking Interferometry

A.L. Gray[1], N. Short, K.E. Mattar and K. C. Jezek

Abstract

Velocities of the Filchner Ice Shelf and its tributary glaciers are derived using a variation of satellite radar interferometry known as speckle tracking. The method requires a coherent pair of SAR passes, a digital elevation model and, for floating ice, an estimate of the height difference due to the tide. Speckle tracking interferometry has the advantage that ice speed and direction can be estimated from one interferometric pair and, with adequate coherence, it is suitable for areas of high velocity and long repeat cycles. Fluxes are estimated using the ice velocities together with ice thickness data derived from a hydrostatic equilibrium model. They are given for gates downstream from the grounding lines of the input tributary glaciers, and for a gate close to the ice shelf edge. The calculations show that the flux close to the edge of the Filchner Ice Shelf (~75.3 km^3/a) is comparable to that estimated further upstream. However, the errors in the estimates (~ 10 km^3/a) preclude any firm conclusions concerning equilibrium of the ice shelf, or bottom surface melt or accretion. Assuming the upstream fluxes reflect the flow across the grounding lines, then the Recovery Glacier is the largest contributor to the ice shelf with 48% and the Slessor Glacier is the second largest with 33%. Support Force Glacier and Foundation Ice Stream both contribute ~7%. Ice Shelf accumulation accounts for the remaining 5%.

Introduction

Ice shelves are huge slabs of ice that extrude from the interior ice sheet onto the polar seas. Almost half of the Antarctic shoreline consists of floating ice shelves (Grosfeld and Gerdes, 1998) and their interaction with the surrounding ocean is the primary means through which Antarctica loses mass. Because ice shelves interact with the ocean and the atmosphere, the time lag with which ice masses normally respond to climate change is considerably shortened. For example, the recently observed collapse of parts of the Antarctic Peninsula Larsen and Wordie ice shelves is concluded to be evidence of regional climate warming (Vaughan and Doake, 1996). Changes in the ice shelves, particularly migration of ice shelf grounding lines (the boundary beyond which the ice is floating), due to changes in ice shelf thickness, may have implications on the rate of ice discharge from the interior ice sheet and hence changes in global sea level. Since Antarctica contains a volume of ice equivalent to 70 m of sea level rise (Hughes, 1998) monitoring Antarctic ice shelves is an important part of climate change studies.

Imagery from the RADARSAT Antarctic Mapping Mission (AMM) is providing a new and detailed view of the morphology and dynamics of Antarctic ice shelves. The AMM took place from September 19 to October 14 in 1997 (Jezek *et al.*, 1998a, b; Jezek, 1999). The mission was a collaboration between the National Aeronautics and Space Association (NASA) and the Canadian Space Agency (CSA) to map Antarctica using the synthetic aperture radar (SAR)

[1] A.L. Gray is with the Canada Centre for Remote Sensing (CCRS), 588 Booth St., Ottawa K1A 0Y7. Tel: (613) 995-3671, fax: (613) 947-1383, email: laurence.gray@ccrs.nrcan.gc.ca.
N. Short works at CCRS for Intermap Technologies under contract to CCRS. K.E. Mattar is with the Defence Research Establishment, 3701 Carling Ave., Ottawa, K1A 0Z4 and K.C Jezek is with the Byrd Polar Research Center, The Ohio State University, 1090 Carmack Road, Columbus, OH 43210, USA.

aboard the Canadian satellite RADARSAT. Rotation of the satellite from normal right looking to a left looking mode enabled the first complete, high resolution mapping of the continent. The first results of the AMM were a SAR amplitude map produced by the Byrd Polar Research Center (BPRC) and termed the Antarctic Mosaic. As RADARSAT has a repeat orbit of 24 days and the AMM lasted for 30 days, the final 6 days of the mission were used to collect repeat data suitable for interferometry (Jezek *et al.*, 1998a; Jezek, 1999). Results from interferometric studies are now becoming available.

Repeat-pass SAR interferometry is well established as a means for measuring glacial ice motion (Goldstein *et al.*, 1993; Joughin *et al.*, 1995, 1996, 1999a; Kwok and Fahnestock, 1996; Rignot, 1996; Mohr *et al.*, 1998, Frolich and Doake, 1998, Dowdeswell *et al*., 1998, Fatland and Lingle, 1998, Stenoien and Bentley, 2000). Traditional interferometry uses differential phase to calculate radial displacement of a specific surface pixel away from or towards the SAR. While the accuracy of measurement is a fraction of a wavelength (5.6 cm for RADARSAT), the velocity information is limited to the range direction unless some assumption is made concerning flow direction. Using both ascending and descending image pairs can improve the information on ice motion direction (Kwok and Fahnestock, 1996; Joughin *et al.*, 1998; Mohr *et al.,* 1998; Vachon *et al.*, 1998). The interferometric method used here is a refinement of the image registration stage in phase interferometry. It eliminates the range only directional limitation imposed by the use of phase by using the correlation of image speckle (Gray *et al.*, 1998). Often referred to as "speckle tracking", the method uses the cross correlation of small 'chips' of SAR imagery to determine flow direction and speed. Similar methodologies have been successfully applied by Thiele *et al.* (1996), Michel and Rignot (1999), Derauw (1999) and Joughin *et al.* (1999b).

This paper describes the speckle tracking methodology and presents the first detailed measurements of surface velocity obtained for the Filchner Ice Shelf. Combining these velocities with estimates of ice shelf thickness we quantify the ice flux at gates ~ 20 km downstream from the input glacier grounding lines and for a gate close to the ice front.

Study area

The Filchner Ice Shelf (FIS) is located in the southern embayment of the Weddell Sea, it forms the eastern arm of the Filchner-Ronne Ice Shelf, between Berkner Island and Coats Land. The ice shelf is fed by tributary glaciers from East Antarctica (McIntyre, 1986) and is thus important in the stability of the eastern sector of the continent. It is also the source of huge tabular ice bergs that calve periodically into the Weddell Sea and a potential factor in the formation of Antarctic Bottom Water which in turn plays a key role in global thermohaline circulation (Foldvik *et al.*, 1985; Hellmer and Olbers, 1991; Gammelsrød *et al.,* 1994; Mikolajewicz, 1998).

The velocity of specific points on the ice shelf has been studied since the 1950s using a variety of techniques. The results vary and often lack any quantification of error. Table 1 summarizes the results of these studies. Vaughan and Jonas (1996) summarized the early velocity estimates for the Filchner Ronne Ice Shelf and their work shows the sparsity of data in this area, particularly for the Filchner Ice Shelf.

Table 1: Velocity estimates from a variety of locations on the Filchner Ice Shelf

Technique	**Velocity**	**Reference**
Astronomical positioning	1300 and 2500 m/a 1242 m/a	Aughenbaugh *et al.,* 1958 Lisognoli, 1964
Temperature studies	2000 m/a	Wexler, 1960
Ice front positions in ERTS-1 imagery	644, 721, 1194, 1460 and 1762 m/a (increasing westward across the front)	Colville, 1976
Doppler satellite measurements	1400 m/a 1059 m/a	Crabtree and Doake, 1980 Gerdau and Schenke, 1984
Ice front advance rates from observation	< 2000 m/a 1000 to 1200 m/a westward across the ice front	Orheim, 1979 Lange and Kohnen, 1985
Tandem mode ERS interferometry	890 m/a, 1163 m/a increasing westward to < 1450 m/a	Schmidt *et al.*, 1999
Ice shelf/ocean model	1200 m/a at ice front	Grosfeld *et al.*, 1998

Estimates of flux have also been made since the 1960s and are summarized in Table 2. For consistency and ease of comparison all estimates are quoted here in km^3/a of ice, using a density of 850 kg/m^3 (Lange, 1987) for the conversion where necessary.

Table 2: Estimates of ice flux

Location	**Flux (km^3/a)**	**Reference**
FIS ice front	120	Behrendt, 1962
〃	127.1 ± 47	Giovenetto, 1970
〃	82	Doake, 1985
〃	70.2	Lange, 1987
〃	70.6	Bentley and Giovenetto, 1991
Foundation Ice Stream	4.0 ± 2.5	Lambrecht *et al.,* 1998
Sum of fluxes from the drainage basins of Slessor, Recovery, Support Force and Bailey.	118	McIntyre, 1986

Behrendt's (1962) original estimate of 120 km^3/a for the FIS used a width of 240 km, an average velocity of 2 km/a and an average ice thickness of 250 m. Maps derived from Landsat satellite imagery since that time (Vaughan *et al*., 1995) show that the current ice front of the FIS is ~160 km wide and so this early estimate certainly exaggerates the current flux. The flux estimate of Doake (1985) was made just prior to the major calving event of 1986 and used an ice front width of 180 km, again wider than the present width. The flux estimates by Lange (1987) and Bentley and Giovenetto (1991) have utilised more recent Landsat data and observations of the ice front to determine ice speed and front width and are likely to be closer to the current value. The estimate

for the Foundation Ice Stream (Lambrecht *et al.* 1998) was calculated using a combination of field data and numerical modelling. Balance velocities and basin accumulation were modelled by McIntyre (1986) to estimate ice discharge into the Filchner Ronne Ice Shelf.

It is interesting to note that the relatively high balance velocity estimated for the Bailey Ice Stream (275 m/a) in McIntyre (1986) appears consistent with the Antarctic wide estimates illustrated in Figure 2 of Bamber *et al.*, (2000), but not with the lower velocities derived in the present work. Most of the present data is downstream of the grounding line but even here the speeds are only ~150 m/a. As the Bamber *et al.*, (2000) work reflects recent, reliable ice topography from ERS altimetry, this discrepancy suggests that this part of the Filchner drainage system may not be in equilibrium.

InSAR methodology for ice velocity

In our original assessment of five interferometric pairs completed soon after the AMM, it was clear that there were areas with sufficient coherence for study, but that traditional interferometric techniques dependent on the differential phase would be difficult to apply. The reasons for this were:

- For the 6 day AMM InSAR mission (Crawford, 1997; Jezek, *et al.,* 1998a) most of the interesting areas were covered by only an ascending or a descending pair so that a solution for 2-dimensional ice motion would be impossible from phase alone.
- Phase unwrapping would be difficult because of the very high fringe rate caused by the long 24 day period between acquisitions, coupled with the high flow rates and patchy coherence in many scenes.

As a result of these considerations it was decided to develop a 2-dimensional image chip or patch correlation technique. When the backscatter from an area remains coherent, then the image speckle pattern will be correlated and it is possible to register patches from the 2 images to a small fraction of a pixel spacing. It should be emphasized that this does not depend on image features. In fact, use of this 'speckle tracking' technique is normally much more accurate than any type of incoherent image feature tracking procedure.

The advantages of the speckle tracking technique are:

- Motion in both the range and azimuth direction can be derived.
- No phase unwrapping is required so that velocity can be derived for areas separated by incoherent data.
- Assuming coherence, the speckle tracking technique will work for high ice speeds and longer orbit repeat cycles.
- If the topography and satellite orbits are known accurately, then the ice speed can be derived from the range and azimuth displacement data in a straightforward manner. In practice however, the uncertainty in both the ice topography and satellite orbit data is such that ice velocity 'control' is still required to calibrate the ice speed.

The disadvantages of the speckle tracking technique are:

- The relative velocity in range is much less accurate with speckle tracking than with unwrapped differential phase. To estimate the range displacement to an accuracy of 0.5 m

(1/50 of a 25 m range pixel) would require good coherence and averaging over a relatively large area (Bamler, 1999). However, the resulting estimate would still be at least an order of magnitude worse than that possible with differential phase. For this reason, it is recommended that wherever possible, differential phase also be used for the range component of the ice motion. Experience has shown, however, that often the use of differential phase for radial motion from RADARSAT data is limited to areas with lower ice speeds, typically less than ~125 m/a. For many Antarctic glaciers speeds exceed 300 m/a, and the gradients in speed can also be high, thus making the use of differential phase difficult for 24 day repeat RADARSAT or 35 day repeat ERS-2 data.

Ice velocity can be estimated from the corrected range and azimuth displacements using the formalism given by Joughin *et al.* (1996), see Figure 1. The range (δ_r) and azimuth (δ_a) displacements can be related to the displacements in a local Cartesian co-ordinate system (δ_x parallel to the azimuth direction, δ_y locally horizontal and parallel to the range plane, and δ_z local vertical) by

$$\delta_r = B_p + \delta_y \sin\theta - \delta_z \cos\theta \qquad (1)$$

$$\delta_x = \delta_a \qquad (2)$$

where:

$B_p = B\cos(\chi - \alpha)$ is the parallel baseline, see Figure 1.

α = look angle at the satellite

θ = local incidence angle

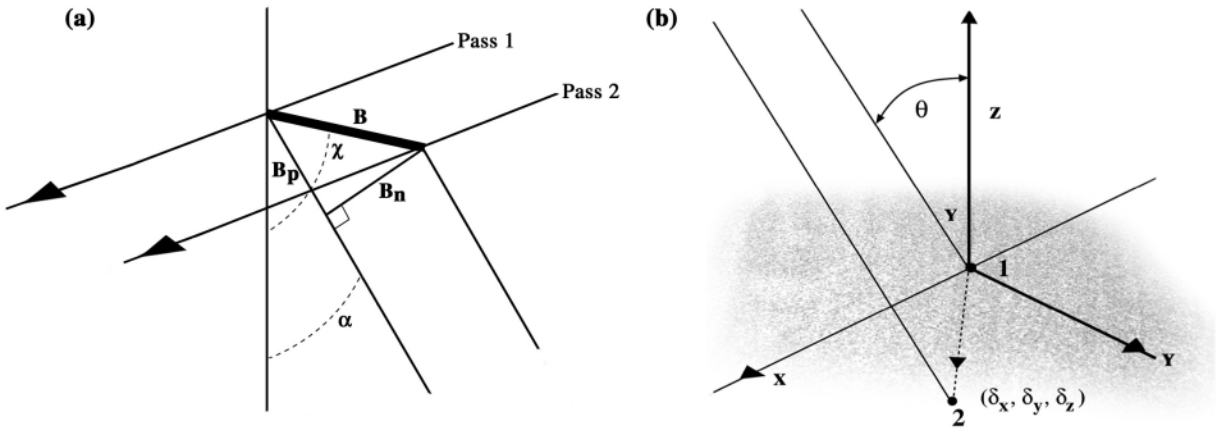

Figure 1: Illustration of (a) satellite geometry and (b) ground geometry for the calculation of surface displacement in three dimensions. B is the baseline, B_p is the parallel baseline and B_n is

the perpendicular baseline, χ is the baseline angle, α is the radar look angle at the satellite, and θ is the local incidence angle. In (b), the yz plane is in the plane of incidence and x is parallel to the along-track direction. The displacements of the ice between the times of the 2 passes are described in this frame by $(\delta_x, \delta_y, \delta_z)$.

Assuming that the ice motion is parallel to the ice surface then the vertical displacement can be related to the horizontal displacements through (Joughin *et al.,* 1996):

$$\delta_z = \delta_x S_a + \delta_y S_r \tag{3}$$

Where S_a and S_r are the local azimuth and range slopes. The approximations implicit in this assumption have been discussed by Reeh *et al.* (1999). In the present context, the additional error associated with the 'surface parallel' approximation is negligible. From these equations one can derive the local horizontal displacement in the range plane as:

$$\delta_y = \left(\delta_r - B_p + \delta_a S_a \cos\theta\right)/\left(\sin\theta - S_r \cos\theta\right) \tag{4}$$

The total ice displacement is then $\delta = \sqrt{\delta_x^2 + \delta_y^2 + \delta_z^2}$, and the ice velocity, V , in meters per year is:

$$V = (365/24)\delta \tag{5}$$

where the factor (365/24) reflects the 24 day RADARSAT repeat orbit. Strictly speaking, this factor should reflect the solar year, i.e. (365.2425/24), but the difference is small. The direction of motion can be estimated readily from δ_x and δ_y , and the angle between the local azimuth and true north.

The SAR data processing steps to produce the estimates of range and azimuth displacement are summarized in Figure 2. The procedure for combining the elevation data, the tidal model and the orbit information with the displacement data, first to correct the displacement data and then to estimate ice speed, is given in Figure 3.

The azimuth displacement correction mentioned in the first box of Figure 3 requires some extra explanation. The basic azimuth spacing between pixels is a function primarily of the radar pulse repetition frequency (*prf*), but also depends on orbit height, terrain elevation, radar look angle and on latitude dependent Earth rotation parameters, see for example Raney (1986). For an interferometric pair the Earth rotation, topographic contributions, *prf*, etc., are the same, but there remains the subtle difference in azimuth pixel spacing as a function of the differences in the 2 orbits, i.e. the baseline. From a straightforward consideration of the geometry (assuming a circular orbit), and the variation in satellite speed with distance *H* from the centre of the Earth, it is possible to show that the fractional change in the azimuth pixel spacing is given by:

$$\left(\rho_{az1} - \rho_{az2}\right)/\rho_{az1} = \left(-1.5B_V + B_H \tan\phi\right)/H \tag{6}$$

where:

$\rho_{az1,2}$ = the azimuth pixel spacing for passes 1 and 2, neglecting Earth rotation effects.

$\left(\rho_{az1} - \rho_{az2}\right)$ = the difference in azimuth pixel spacing.

B_V = the vertical baseline (positive for pass 2 higher than pass 1).

B_H = the horizontal baseline (positive when the angle ϕ subtended at the centre of the Earth by the sub-satellite point and the swath pixel decreases for pass 2 in relation to pass 1).

For example, for a purely vertical separation of the orbits equivalent to a change of 2 parts in 10^6 of the orbit radius (corresponding to ~ 14 m change in satellite height), the azimuth spacing will change by 3 parts in 10^6. In this case there will be an accumulating azimuth displacement such that after 10^5 pixels (~ 500 km) there will be a relative azimuth displacement of 0.3 pixels, which is easily measurable. However, this correction may not be necessary if there are along-track velocity control areas.

The correction to the range displacement data due to tidal motion has been made using an Antarctic tidal model (Padman *et al.*, 2000; Rignot *et al.*, 2000) to predict heights at the times of the satellite overpasses. The predictions were provided to us by L. Padman and showed that height differences of 2 – 2.5 m were quite common across the FIS. The tidal height difference data were resampled to the same grid as the estimates of ice motion, a mask was generated to identify those values on floating ice, and the range displacement was corrected by projecting the vertical motion due to the tide in the direction of the SAR. The position of the grounding zone was estimated, where possible, by examining the phase fringes from the interferometric SAR data (Goldstein *et al.,* 1993, Rignot, 1996). In the region close to the grounding zone, within 5-10 km, the range displacement offset was reduced according to the model of ice shelf flexing used by Goldstein *et al.* (1993).

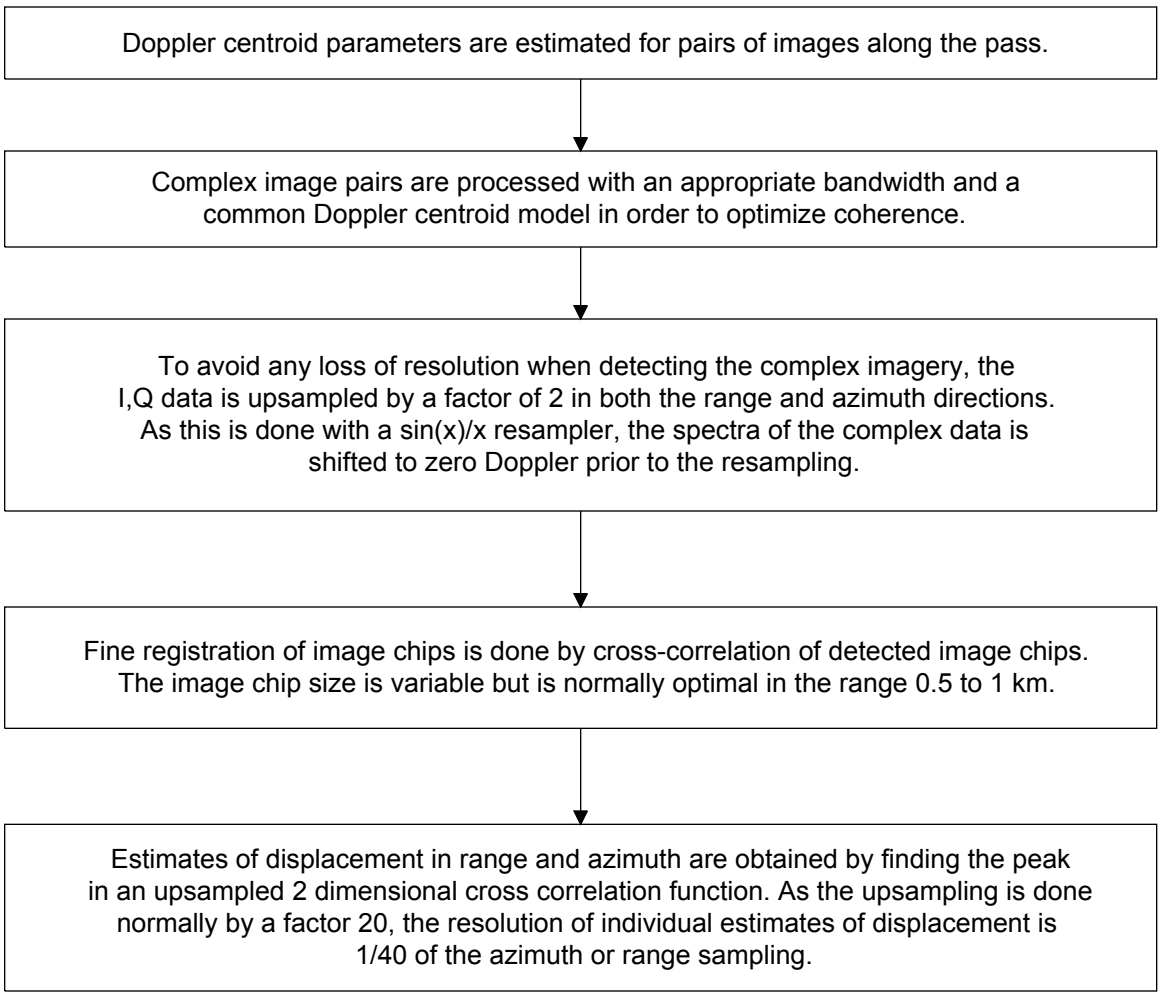

Figure 2: Data processing sequence to generate azimuth and range displacement data.

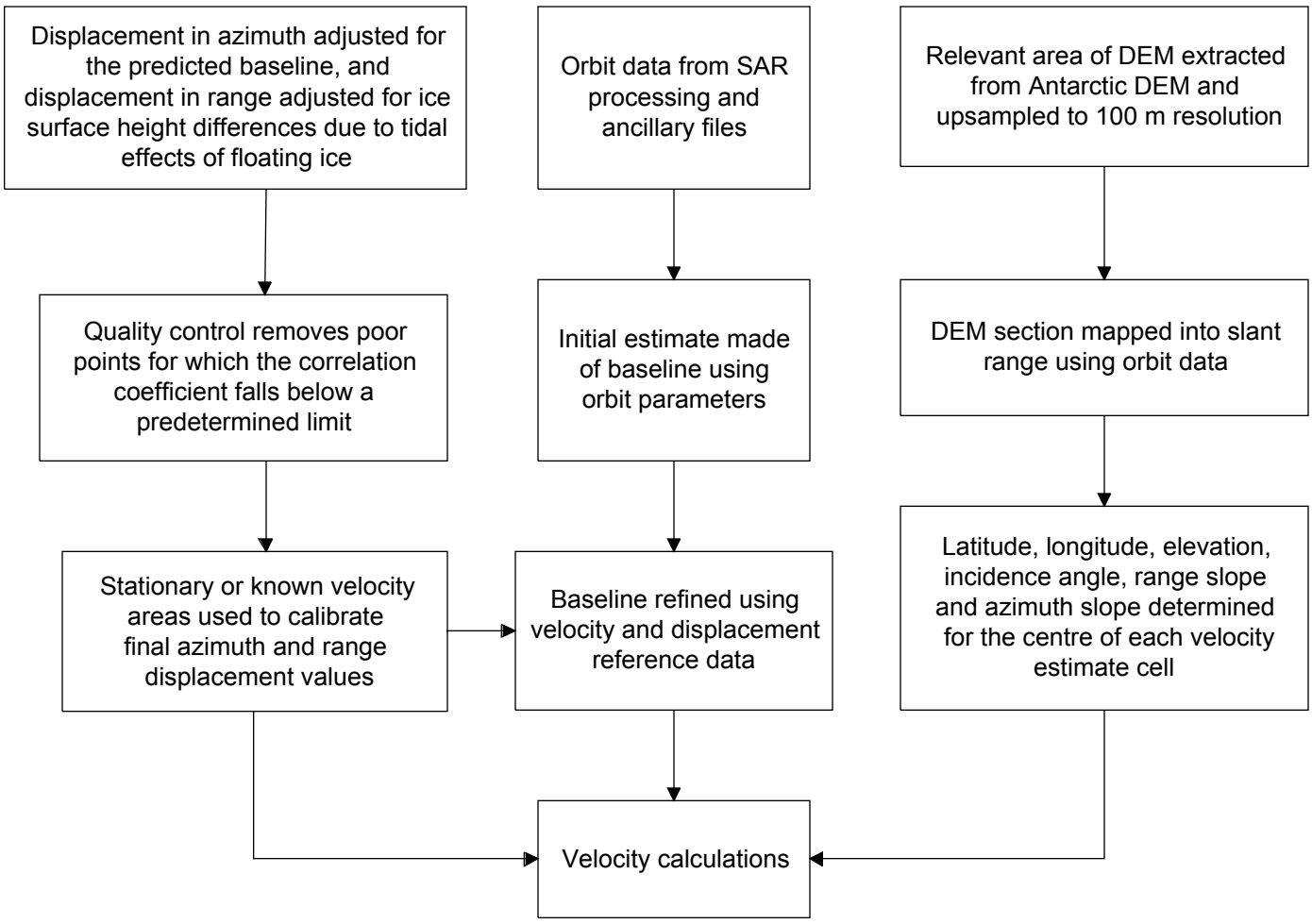

Figure: 3 Procedure for velocity calculations based on the DEM, orbit and displacement data.

Errors in the speckle tracking approach

The uncertainty in velocity, ΔV, arises from both random and bias errors in the displacement estimates. In general, the uncertainty in velocity is related to the uncertainty in the displacement estimates, $\Delta\delta_x$, $\Delta\delta_y$, and $\Delta\delta_z$, by:

$$\Delta V = \left[c^2 \delta_x / V \right] \Delta\delta_x + \left[c^2 \delta_y / V \right] \Delta\delta_y + \left[c^2 \delta_z / V \right] \Delta\delta_z \qquad (7)$$

where:

$c = 365/24$

The last term can be neglected as the vertical motion is normally much smaller than the horizontal motion.

Random errors

The standard deviation or random component of the uncertainty in an estimate of displacement in 'speckle tracking' has been given by Bamler (1999) as:

$$\sigma_{\delta_{x,y}} = \sqrt{\frac{3}{2N}} \frac{\sqrt{1-\gamma^2}}{\pi\gamma} osf^{3/2} \rho_{x,y} \qquad (8)$$

Where:

$\sigma_{\delta_{x,y}}$ = standard deviation of the estimate of displacement in the x or y direction (has same units as pixel spacing).

N = number of samples in each registration window

γ = coherence

osf = oversampling ratio

$\rho_{x,y}$ = pixel spacing (m)

Typically, we use N = 1.2×10^4 samples in the registration window, and γ is usually between 0.3 and 0.6. The oversampling factor in range is around 1.2, but depends on the processed bandwidth in azimuth. Typically, the product of the range and azimuth oversampling is around 2.

From (8) above, the random component in the speckle tracking component for an individual estimate of azimuth displacement is in the range 1.1 to 2.6 m/a. The unit of displacement in our work has usually been 1/40 of a pixel spacing which corresponds to a velocity quantization of ~ 2 m/a in azimuth (ρ_x □ 5.4 m), so that for individual estimates the quantization may limit the accuracy. In fact, further averaging is normally done and this would rarely limit final accuracy.

In the range plane, the errors from speckle tracking are more significant than those in azimuth. As the pixel sampling in ground range, ρ_y, is ~ 20 m in (8) above, the random error in an individual estimate of registration in the speckle tracking process in the range direction is in the range 4 to 10 m rms. Again, by averaging the results over a 5 x 5 km window the random component of error can be further reduced and is normally much smaller than bias errors.

Bias errors

The first source of bias errors in azimuth is uncertainty in along-track registration. Velocity reference control is needed in the azimuth direction to correct for this uncertainty. This is best obtained by identifying regions of zero or known velocity on low slope terrain. Any error in this value translates directly into a bias error in the results. Unfortunately, even if a good control point can be identified, a bias error may still enter into the results as one moves further away from the reference point. This can arise because of small errors in the orbit models. For example, the orbit models may be incorrect such that the assumed zero Doppler direction may not be precisely correct, i.e. in the interferogram there may be an uncompensated squint, leading to a range dependent displacement in azimuth bias. Although these errors are very small, over long distances they can become a significant fraction of an azimuth pixel spacing. As a result, it is desirable to have both along- and across-track control, preferably separated by less than 100 km. It is difficult to quantify these errors and they have to be treated on a pass-by-pass basis.

The second source of errors in speckle tracking for displacement in azimuth arises from the possibility of a varying electron density in the ionosphere. Evidence has been presented (Gray *et al.*, 2000) that along-track variations in electron density can affect satellite SAR through both phase errors and a mismapping of pixels in azimuth. The effect has been observed previously in ERS satellite radar interferometry (e.g. Joughin *et al.,* 1996), particularly in data collected in the polar auroral zones. For C-band interferometry the effect appears as 'streaks' in an image of the azimuth displacement, where the streaks are aligned close to the range direction. For the C-band satellite SAR data, the modulation in azimuth displacement is on a 1 km scale in the azimuth direction, and the amplitude is typically in the range 0.1 to 0.2 of a pixel spacing. At L-band both the depth of modulation and width of the streaks in azimuth are larger, which will make the application of this technique potentially more difficult at this frequency. The azimuth displacement due to this ionospheric effect can lead to serious errors in velocity (~ 10 m/a or more at C-band), however, filtering over along-track distances of approximately 5 km can be used to reduce the modulation. The effect has been observed with the RADARSAT AMM InSAR data, but the passes from which these ice flux results have been derived were not corrupted by this effect.

Bias errors in displacement in the range plane can arise from errors in baseline estimation, errors associated with the displacement calibration, errors in tidal corrections for floating ice, and DEM errors. These errors have been discussed in the literature, see e.g. Joughin *et al.* (1996) and Frolich and Doake, (1998). If, for example, a near swath reference velocity is used then an error in either the baseline model or the DEM at that point is unimportant as the parallel baseline has been corrected to compensate for the problem. However, at other points in the scene, particularly at other radar look angles, there will be an error dependent on the error in the DEM, the magnitude of the perpendicular baseline, and the error in the baseline model. Joughin's conclusion (Joughin *at al.,* 1996) that baseline error is often the largest source of error in the estimation of ice velocity from differential phase is also true for the speckle tracking method.

It is useful, however, to look at the magnitude of some of the contributions particularly because of the longer orbit repeat cycle of RADARSAT (24 days) in relation to the early ERS-1 (3 days) or ERS tandem mode (1 day) data. An error of 100 m in terrain height, coupled with a perpendicular baseline of 100 m will lead to a bias error in velocity of only around 1 m/a, dependent on the mode of data acquisition (the error reduces slightly for the larger incidence angle modes). However, the error in knowledge of the parallel baseline can be more significant: even if a good velocity reference area exists at one point in the swath this only calibrates the parallel baseline at that incidence angle, and the error at other points in the swath will lead directly to a bias error. For example, at 30 degrees incidence a 0.5 m error in parallel baseline leads to an error of around 15 m/a in estimated ice speed in the ground range direction. This can be the most serious error in the estimation of ice velocity and it reinforces the desire to have as much reference data as possible, particularly near and far range, so that the baseline can be refined.

For regions of floating ice, an incorrect compensation for the vertical tidal motion will cause an additional bias error for the range component of horizontal motion (Rignot, 1996). As explained earlier, the variation in the range displacement due to tide related height variation between image acquisitions is removed using results from an Antarctic tidal model (Padman *et al.*, 2000; Rignot *et al.*, 2000). Potential errors can arise in the sub-shelf tidal model because of poor bathymetry and mismapped grounding lines. Estimated model errors due to these and other errors are in the 10-50 cm range (Padman, 2000). In addition, the height over floating ice can be influenced by

the "inverse barometric effect" or "IBE" (Gill, 1982; Rignot *et al.*, 2000). The IBE involves a depression of ~1 cm of the sea surface (and floating ice) for each 1 millibar increase in atmospheric pressure: the pressure anomaly for a typical polar low is ~30 millibars, so the IBE error in height can be ~30 cm. As the RADARSAT passes are separated by 24 days, the atmospheric pressures from separate passes are essentially decorrelated and it is quite possible that atmospheric pressures could lead to a significant height difference regardless of the accuracy of the tidal model. A 20 mb pressure change can lead to a height change of ~20 cm (Padman *et al.*, 2000), which if uncompensated would lead to a cross-track velocity error of around 5 m/a. Barometric pressure data were obtained from the British Antarctic Survey, Halley Station on the Brunt Ice Shelf (~ 500 km from the middle of the FIS). The barometric pressure differences at the overpass times of the 2 pairs of data covering the floating ice were quite low, in one case less than 1 mb and in the other case ~7 mb, so it is unlikely that a significant error has arisen from this effect.

Data

The FIS area is covered with three swaths of interferometric RADARSAT data. Figure 4 shows the location of the study area and the coverage of the data. The swath descriptions are given in Table 3.

Table 3: Swath descriptions

Swath	Mode	Incidence angle	Parallel baseline (m)	Perpendicular baseline (m)	Acquisition dates
A	S7	44 - 49º	184.3	261.8	21/9/1997 and 15/10/1997
B	S2	24 - 31º	53.6	121.6	24/9/1997 and 18/10/1997
C	S2	24 –31º	83.7	197.2	23/9/1997 and 17/10/1997

Swath A, covering the upstream sections of the Recovery and Slessor Glaciers is standard 7 mode, with incidence angles varying from 44 to 49º from near to far range. Swaths B and C, which cover the FIS are standard 2 mode, with incidence angles varying from 24 to 31º from near to far range. The baselines are nominal values given for mid-swath, mid-range.

Surface elevations were obtained from the Antarctic digital elevation model (DEM) compiled by the Byrd Polar Research Center (BPRC) of The Ohio-State University (Jezek *et al.*, 2000). For the study area, most elevations were originally derived from satellite altimeter data.

Tidal corrections for the ice shelf were performed using predictions from an Antarctic tidal model, as discussed above.

Figure 5 illustrates the ice surface velocity for the 3 swaths as a colour overlay on the AMM mosaic. The low speeds are represented with blue tones, changing to red and purple for the highest speeds.

Surface accumulation rates from Graf *et al.* (1988) and Oerter *et al.* (1998) were used to create a local accumulation data set using average accumulation values for the latitude of the ice shelf. These rates were originally derived from accumulation depths in snowpits on the ice shelf surface and show a steady decline from 24 g/cm^2/a at the ice front to 13.7 g/cm^2/a at the

grounding line. They are considered accurate to 20% due to wind erosion and snow redistribution.

Ice thickness

In order to calculate ice flux, velocities must be combined with ice thickness data. It is possible to derive ice shelf thickness using the principle of regional hydrostatic equilibrium if the ice surface elevation is known. Ice thickness data have been calculated for the FIS using the surface elevations from the BPRC DEM and the relationship derived for the adjacent Ronne Ice Shelf by Vaughan *et al.* (1995), which is:

$$h = 0.108H + 17 \qquad (9)$$

where:

h = surface elevation (referenced to OSU91 geoid model) (m)
H = total ice thickness (m)
17 = correction for lower firn density and offset between geoid model and true sea level (m)

The equation is considered reliable to ±70 m in ice thickness.

Flux calculations

Gates were taken across the ice shelf downstream from the entry of the tributary glaciers into the FIS. While it is desirable to estimate the input flux from each glacier, uncertainty about the exact grounding line position and the desire to use the hydrostatic equilibrium principle in the calculation of ice thickness led to the downstream choice. The gates were placed ~ 20 km downglacier of the estimated grounding line. The 3-dimensional circulation model of Grosfield et al., (1998) indicated basal melting of ~ 1 m/a in the grounding line region of both the Recovery and Slessors Glaciers, for this reason it is acknowledged that the gate fluxes may underestimate the actual input fluxes. Gate width is constrained by the flow stripes, assumed to represent flow direction. The interferometrically derived flow directions are seen to agree well with the flow stripes suggesting stable and consistent patterns of flow over the last 500 years. The ice front gate is placed at the northern limit of the data, as close as possible to the actual ice front. Gates across the tributary glaciers are placed 300 years of flow back from the ice front gate (on the assumption that there has not been a significant change in flow in this period). The time delay between gate positions was determined using an integration of the velocity and distance along the flow stripes. Figure 4 shows the positions of the gates and the flow stripe profiles used to determine the 300 year limit in yellow.

As velocity and ice thickness vary across the gate, each gate is sub divided into 500 m sections and the flux calculated as the sum of the subsection fluxes. The summation has used subsection widths estimated perpendicular to the flow direction, determined using the interferometrically derived flow direction.

$$\sum_{i=1}^{N} H_{x_i} \times W_{x_i} \times V_{x_i} \quad (10)$$

Where:
H = thickness (m)
V = velocity (m/a)
W = section width (m) perpendicular to the flow direction
$x_{i...N}$ = gate section

The contributions of ice from the Bailey Ice Stream and Berkner Island are not included in either the ice front or upstream gates due to potential thickness inaccuracies caused by the proximity to grounded ice, and the difficulty of velocity estimation in the high shear regions at the eastern and western edges of the Filchner Ice Shelf.

The area contained within the gates and profiles is multiplied by the local accumulation rate to calculate the annual volume of surface accumulation in the FIS study area. An error estimate of ± 20% is associated with the accumulation volume.

Flux calculation errors

As the derived flow directions and flow stripes are consistent for the ice shelf and inland thereof, we are confident that the pattern of flow from the major input glaciers has remained relatively constant over the past five centuries. We assume therefore that the gates are representative of the width of the tributaries in the ice shelf. The dominant error associated with the gate velocity profile is that associated with the determination of reference velocities. This is estimated for each pass and then the error in velocity and ice thickness is combined as follows to estimate the flux error. The maximum flux is estimated by combining the gate velocity profile plus the associated error in velocity, with the ice thickness profile plus the associated error in thickness. Similarly, the minimum flux value is estimated by combining the velocity profile minus the estimated velocity error with the ice thickness minus the estimated thickness error. Using areas from Berkner Island, the Shackleton Range, the Whichaway Nunataks and the areas adjacent to the provisionally named Blackwall Ice Stream as low speed reference areas, we estimate the velocity error to be ± 21 m/a. The error in ice thickness is taken as ± 70 m (Vaughan *et al*., 1995). These calculations are made for each gate subsection and summed for the final minimum and maximum gate flux estimates.

The largest errors in flux are associated with the northern, 'ice front', gate. Some velocity control is provided by the relatively slow moving ice of Berkner Island on the west and Coats Land on the east, as well as the mountains on both passes further to the south. Although the random errors are larger for the ice front gate, due to increased noise in the fine registration of the image chips, the potential bias errors still dominate. In addition, there is a section of the gate (coloured red in Figure 6c) for which the data has been interpolated using a polynomial fit to span across the data gap. To account for these problems we have used a relatively high velocity error of ± 30 m/a and a thickness error of ± 70 m in estimating the flux limits for the ice front.

Results

Figure 5 shows the derived velocities as a colour overlay on the amplitude mosaic. The spatial distribution and range of velocities agrees well with others, in particular the trend of westward increasing velocities noted by Lange and Kohnen (1985) and Schmidt *et al.* (1999). The velocity data also confirm the existence of two new ice streams first identified in the Antarctic Mosaic by Jezek (1999). These ice streams actively feed the Recovery Glacier and their velocities of between 200 and 400 m/a can be seen in Figure 5. They have been provisionally named the RAMP Ice Stream, after the RADARSAT Antarctic Mapping Project, and the Blackwall Ice Stream, after Hugh Blackwall Evans, the first Canadian scientist to work and overwinter in Antarctica in 1899.

Figure 6 illustrates the velocity variation across the Recovery (6a) and the Slessor gates (6b), and the ice front (6c). Figure (6a) is for gate R1 in Figure 4. The blue lines are based on the velocity estimates and the red sections in Figure 6a and 6c are interpolated. For the ice front gate (6c) there is a central section of missing velocity data due to the non-overlapping image swaths. For this area the ice velocities are interpolated between the real values of the swaths either side. Interpolation using polynomial fitting is also used to provide estimates of velocity over the areas where there is loss of coherence such as the shear margins.

Table 4: Flux results (See Figure 4 for gate positions and Figure 6 for profile examples)

Input source	**Minimum flux (km^3/a)**	**Flux (km^3/a)**	**Maximum flux (km^3/a)**	**Percentage contribution**
Recovery Glacier	30.4	34.9	39.7	47.4
Slessor Glacier	20.5	24.0	27.3	32.6
Support Force Glacier	4.6	5.4	6.2	7.4
Foundation Ice Stream	4.4	5.3	6.2	7.2
Accumulation	3.2	4.0	4.7	5.4
Total input	**63.1**	**73.6**	**84.1**	**100.0**
Ice front **Total output**	**64.2**	**75.3**	**87.0**	

The fluxes show that the Slessor and Recovery Glaciers are the most important contributors to the FIS, together accounting directly for 80% of the ice volume. This dominant role of the Recovery and Slessor Glaciers in the ice shelf flux indirectly highlights the importance of their catchment areas in East Antarctica and the possible changes that may result from a climatically induced reduction in the size of the ice shelf. The flux of Foundation Ice Stream (5.3 ± 0.9 km^3/a) is found to match reasonably with the estimate of 4 ± 2.5 km^3/a by Lambrecht *et al.* (1998). In the total estimate above no contribution has been included from Coats Land or the Bailey Ice Stream on the east or from Berkner Island on the west of the FIS, because of uncertainties in the ice thickness and speed. However, the contribution appears to be quite low and would only increase the total flux by ~5%.

While the similar input and output ice volumes imply that the ice shelf is not dramatically out of equilibrium, the associated errors are large and we do not know the scenario at the ice shelf edge and at the grounding line, areas where considerable melting usually takes place. Grosfeld *et al.* (1998) proposed an average melt rate of 0.35 m/a for the FIS but showed that it was spatially variant with some regions close to Berkner island actually experiencing refreezing of < 2.8 m/a.

While we are currently unable to comment on this proposed regime, the acquisition of accurate thickness data in the grounding line regions, and interferometric coverage of the northern ice edge, would enlarge the present study and enable the investigation of basal melt and accretion rates, and improve our knowledge of the equilibrium status of the ice shelf.

Conclusions

Speckle tracking interferometry is an effective and useful technique for monitoring Antarctic ice motion. The method has advantages for areas of high velocity and long repeat cycles and is particularly suitable for the large, flat surfaces of ice shelves. When used for ice shelf monitoring the method requires the additional input of tidal height variations between image acquisitions. Areas of stationary ice or mountains are needed to correct for bias errors in the speckle tracking method. Interferometrically derived velocities are especially useful when combined with ice thickness data and used to calculate ice flux. For the FIS we show that the Slessor and Recovery Glaciers dominate the regime of the ice shelf, directly contributing ~ 80% of the ice shelf volume. Because the flow stripes are parallel to the ice velocity vectors and there are similar fluxes in the FIS at gates separated by a distance equivalent to ~ 300 years, we suggest that the flow regime in the FIS has not changed dramatically in the last few hundred years.

Acknowledgements

The RADARSAT data was provided by Radarsat International (RSI) and is copyright the Canadian Space Agency. Laurence Padman, Earth & Space Research, generously provided model tidal heights for the times of the 4 RADARSAT passes used over the Filchner Ice Shelf. Rick Forster, University of Utah, and Biyan Li and Zhiyuan Zhao, graduate students at the Byrd Polar Research Center, the Ohio-State University provided useful help and comments at various stages of the work. In particular, we acknowledge the work at BPRC in calculating the Antarctic DEM. Jonathan Bamber also provided a DEM. Eric Rignot, Laurence Padman and Chris Doake provided very helpful comments on the manuscript.

References

Aughenbaugh, N., Neuberg, H., and Walker P. (1958). Ellsworth Station Glaciological and Geological Data 1957-1958, *The Ohio State University Research Foundation Report,* Part 1, pp.825-1.

Bamler, R. (1999). Interferometric Stereo Radargrammetry: Absolute Height Determination from ERS-ENVISAT Interferograms. *Proceedings of IGARSS '99,* Vol 3, (pp. 1517-1521), Hamburg.

Bamber, J.L., Vaughan, D.G., and Joughin, I. (2000), Widespread Complex Flow in the Interior of the Antarctic Ice Sheet, *Science*, 287, pp. 1248-1250.

Behrendt, J.C. (1962). Summary and Discussion of the Geophysical and Glaciological Work in the Filchner Ice Shelf of Antarctica, *University of Wisconsin Research Report Series,* (62-3).

Bentley, C.R. and Giovinetto, M.B. (1991). Mass Balance of Antarctica and Sea-Level Change. In G. Weller, C. Wilson, and B. Severin (Eds), *Proceedings of the International Conference on the Role of the Polar Regions in Global Change*, (pp. 481-488). Fairbanks: Geophysical Institute, University of Alaska,

Colville, A. J. (1976). *Investigation of Fluctuation and Movement of Ice Fronts in the Weddell Sea and Bellingshausen Sea Using Satellite Imagery and Other Data*, M.Sc. Thesis, University of Cambridge.

Crabtree, R. and Doake, C. S. M. (1980). Flow Lines on Antarctic Ice Shelves, *Polar Record*, Vol. 20, No. 124, pp. 31-37.

Crawford, J.P. (1997). Post mission report on data coverage for AMM-1. Presented at the Science Team Meeting Ohio-State University, Nov. 1997.

Derauw, D. (1999). DInSAR and Coherence Tracking Applied to Glaciology: The Example of Shirase Glacier, *FRINGE Meeting 1999*, Liège.

Doake, C.S.M. (1985), Antarctic Mass Balance: Glaciological evidence from Antarctic Peninsula and Weddell Sea sectors. *In Glaciers, Ice Sheets, and Sea Level: Effect of a CO_2 induced Climate Change*, (Workshop Report DC. DOE/ER/60235-1). Washington, U.S. Department of Energy.

Dowdeswell, J.A., Unwin, B., Nuttall, A.M., and Wingham, D.J. (1998). Velocity structure, flow instability and mass flux on a large Arctic ice cap from satellite radar interferometry, *Earth and Planetery Science Letters,* Vol. 167, pp. 131-140.

Fatland, D.R., and Lingle, C.S. (1998). Analysis of the 1993-95 Bering Glacier (Alaska) surge using differential SAR interferometry, *Journal of Glaciology*, Vol. 44, No. 148, pp. 532-546.

Frolich, R.M., and Doake, C.S.M. (1998). Synthetic aperture radar interferometry over Rutford Ice Stream and Carlson Inlet, Antarctica", *Journal of. Glacio*logy, Vol. 44 No. 146, pp. 77-92.

Foldvik, A., Gammelsrød, T., Slotsvik, N. and Tørresen, T. (1985). Oceanographic Conditions on the Weddell Sea Shelf during the German Antarctic Expedition 1979/80, *Polar Research*, Vol. 3, No. 2, pp. 209-226.

Gammelsrød, T., Foldvik, A., Nøst, O., Skagseth, Ø., Anderson, L., Fogelqvist, E., Olsson, K., Tanhua, T., Jones E., and Østerhus, S. (1994). Distribution of Water Masses on the Continental Shelf in the Southern Weddell Sea. In O.M. Johannessen *et al.* (Eds.*), The Polar Oceans and their Role in Shaping the Global Environment, The Nansen Centennial Volume, Geophysical Monograph Series,* Vol. 84, pp. 159-175,Washington D.C.: AGU.

Gerdau, H., and Schenke, H. W. (1984). Doppler-Satellitenbeobachtungen zu Positions- und Bewegungsbestimmungen Deutscher Forschungsstationen in der Antarktis, *Zeitschrift für Vermessungswessen*, Vol. 109, No. 4, pp. 161-175.

Gill, A. E., (1982). Atmosphere-Ocean Dynamics, International Geophysics Series, 30, Academic Press, Inc., San Diego, California, pp. 662.

Giovennetto, M.B. (1970). The Antarctic ice sheet and its bi-modal response to climate*, IAHS Publication* No.86, pp.347-358.

Goldstein, R.M., Englehardt, H., Lamb, B., and Frolich, R.M. (1993). Satellite Radar Interferometry for Monitoring Ice Sheet Motion: Application to an Antarctic Ice Stream, *Science*, Vol. 262, pp. 1525-1530.

Graf, W., Moser, H., Oerter, H., Reinwarth, O., and Stichler, W. (1988). Accumulation and Ice Core Studies on Filchner-Ronne Ice Shelf, Antarctica, *Annals of Glaciology*, Vol. 11, pp. 23-32.

Gray, A.L., Mattar, K.E., Vachon, P.W., Bindschadler, R., Jezek, K.C., Forster, R., and Crawford, J.P. (1998). InSAR Results from the RADARSAT Antarctic Mapping Mission Data: Estimation of Glacier Motion using a Simple Registration Procedure, *Proceedings of. IGARSS '98*, Vol. 3 (pp. 1638-1640), Seattle.

Gray, A.L., Mattar, K.E. and Sofko, G., (2000). Influence of Ionospheric Electron Density Fluctuations on Satellite Radar Interferometry, *Geophysical Research Letters,* Vol. 27, No. 10, pp. 1451-1454.

Grosfeld, K., and Gerdes, R. (1998). Circulation Beneath the Filchner Ice Shelf, Antarctica, and its Sensitivity to Changes in the Oceanic Environment: A Case Study, *Annals of Glaciology*, Vol. 27, pp. 99-104.

Grosfeld, K., Hellmer, H., Jonas, M., Sandhäger, H., Schulte, M., and Vaughan, D. (1998). Marine Ice Beneath Filchner Ice Shelf: Evidence from a Multi-disciplinary Approach, *Antarctic Research Series*, Vol. 75, pp. 319-339.

Hellmer, H. H. and Olbers, D. J. (1991). On the Thermohaline Circulation Beneath the Filchner-Ronne Ice Shelves, *Antarctic Science*, Vol. 3, No. 4, pp. 433-442.

Hughes, T. J. (1998), *Ice Sheets*. Oxford: Oxford University Press.

Jezek, K.C. (1999). Glaciological properties of the Antarctic Ice Sheet from RADARSAT-1 synthetic aperture radar imagery, *Annals of Glaciology*, Vol. 29, pp. 286-290.

Jezek, K.C., Sohn, H.G. and Noltimeir, K.F. (1998a). The Radarsat Antarctic Mapping Project, *Proceedings of IGARSS '98,* Vol. 5 (pp. 2462-2464), Seattle.

Jezek, K.C., Carsey, F., Crawford, J., Curlander, J., Holt, B., Kaupp, V., Lord, K., Labelle-Hammer, N., Mahmood, A., Ondrus, P., and Wales, C. (1998b). Snapshots of Antarctica from RADARSAT-1, *Proceedings of IGARSS '98,* Vol. 3, (pp.1428-1430), Seattle.

Jezek, K.C., Liu, H., Zhao, Z., and Li, B. (2000). Improving a digital elevation model of Antarctica using radar remote sensing data and GIS techniques. *Polar Geography*, Vol. 23, No. 3, pp. 209-224.

Joughin, I.R., Winebrenner, D.P. and Fahnestock, M.A. (1995). Observation of Ice Sheet Motion Using Satellite Radar Interferometry, *Geophysical Research Letters*, Vol. 22, No. 5, pp. 571-574.

Joughin, I.R., Kwok, R. and Fahnestock, M. (1996). Estimation of Ice Sheet Motion Using Satellite Radar Interferometry: Method and Error Analysis with Application to the Humboldt Glacier, Greenland, *Journal of Glaciology*, Vol. 42, No. 142, pp. 10-22.

Joughin, I., Kwok, R., and Fahnestock, M. (1998). Interferometric Estimation of Three-dimensional Ice Flow Using Ascending and Descending Passes, IEEE TGRS, Vol. 36, No.1, pp. 25-37.

Joughin, I., Fahnestock, M., Kwok, R., Gogineni, P., and Allen, C. (1999a). Ice Flow of Humboldt, Petermann and Ryder Gletscher, Northern Greenland, *Journal of Glaciology*, Vol. 45, No.150, pp. 231-241.

Joughin, I., Gray, L., Bindschadler, R., Price, S., Morse, D., Hulbe, C., Mattar, K., and Werner, C. (1999b). Tributaries of West Antarctic Ice Streams Revealed by RADARSAT Interferometry, *Science*, Vol. 286, pp. 283-286.

Kwok, R. and Fahnestock, M.A. (1996). Ice Sheet Motion and Topography from Radar Interferometry, *IEEE TGRS,* Vol. 34, pp. 189-200.

Lambrecht, A., Mayer, C., Oerter, H., and Nixdorf, U. (1998). Mass Balance of the Southeastern Ronne Ice Shelf, Antarctica, *Filchner-Ronne Ice Shelf Programm (FRISP),* (Report No. 12) pp. 45-50. Bremerhaven: Alfred-Wegener-Institut für Polar- und Meeresforschung.

Lange, M. and Kohnen, H. (1985). Ice Front Fluctuations in the Eastern and Southern Weddell Sea, *Annals of Glaciology*, Vol. 6, pp. 187-191.

Lange, M.A. (1987). Quantitative Estimates of the Mass Flux and Ice Movement along the Ice Edges in the Eastern and Southern Weddell Sea. *In Dynamics of the West Antarctic Ice Sheet*, C.J. van der Veen and J. Oerlemans (Eds), Dordrecht: Reidel Publishing.

Lisognoli, C. (1964). Movement of the Filchner Ice Shelf Antarctica, *Transactions, American Geophysical Union,* Vol. 45, No. 2 pp. 391-97.

McIntyre, N. (1986). Discharge of Ice into the Filchner-Ronne Ice Shelves. In H. Kohnen, H. (Ed), *Filchner-Ronne Ice Shelf Programm (FRISP),* (Report No. 3), pp. 47-52, Bremerhaven: Alfred-Wegener-Institut für Polar- und Meeresforschung.

Michel, R. and Rignot, E. (1999). Flow of Glaciar Moreno, Argentina, from Repeat-pass Shuttle Imaging Radar Images: Comparison of the Phase Correlation Method with Radar Interferometry, *Journal of Glaciology*, Vol. 45, No. 149, pp. 93-100.

Mikolajewicz, U. (1998). Effect of Meltwater Input from the Antarctic Ice Sheet on the Thermohaline Circulation, *Annals of Glaciology,* Vol. 27, pp. 311-315.

Mohr, J.J., Reeh, N., and Madsen, S.N. (1998). Three-dimensional Glacial Flow and Surface Elevation Measured with Radar Interferometry, *Nature*, Vol. 391, pp. 273-276.

Oerter, H., Lambrecht, A., Mayer, C., Nixdorf, U., and Graf, W. (1998). Summary of Mass Balance Studies on Möllereisstrom and Foundation Ice Stream, Filchner-Ronne-Schelfeis, Since 1980. In *Filchner-Ronne Ice Shelf Programm (FRISP),* (Report No. 12), pp. 59-64, Bremerhaven: Alfred-Wegener-Institut für Polar- und Meeresforschung.

Orheim, O. (1979). Flow of Antarctic Ice Shelves between Longitudes 29˚E and 44˚W, (abstract), *Journal of Glaciology*, Vol. 24, No. 90, pp. 484-85.

Padman, L., MacAyeal, D. and Rignot, E. (2000). Analysis of Sub-Ice-Shelf Tides in the Weddell Sea Using SAR Interferometry. In *Filchner-Ronne Ice Shelf Programme (FRISP),* (Report No. 13), pp. 60-65, Bremerhaven: Alfred-Wegener-Institut für Polar- und Meeresforschung.

Padman, L. (2000). Personal communication on the ice heights from the tidal height model at the times of the RADARSAT overpasses.

Raney, R.K. (1986). Doppler Properties of Radars in Circular Orbits, *International Journal of Remote Sensing*, Vol. 7, No. 9, pp. 1153-1162.

Reeh, N., Madsen, S.N., and Mohr, J.J. (1999). Combining SAR Interferometry and the Equation of Continuity to Estimate the Three-dimensional Glacier Surface-velocity Vector, *Journal of Glaciology,* Vol. 45, No.151, pp. 533-538.

Rignot, E. (1996). Tidal Motion, Ice Velocity and Melt Rate of Petermann Gletscher, Greenland, Measured by SAR Interferometry, *Journal of Glaciology*, Vol. 42, No.142, pp. 476-485.

Rignot, E., Padman, L., MacAyeal, D.R., and Schmeltz, L. (2000). Observation of Ocean Tides beneath the Filchner Ronne Ice Shelf using SAR Interferometry: Comparison with Tidal Model Predictions, *Journal of Geophysical Research*, 105, (C8), pp. 19615-19630.

Schmidt, J., Thiel, K-H., and Sandhäger, H. (1999). Large Scale Interferometry over Filchner-Ronne Ice Shelf, *FRINGE Meeting 1999*, Liège.

Stenoien, M.D. and Bentley, C.R. (2000). Pine Island Glacier, Antarctica: A study of the catchment using interferometric synthetic aperture radar measurements and radar altimetry, *Journal of Geophysical Research*, 105, (B9), pp. 21761-21779.

Thiele, K.H., Wehr, A., Wu, X., (1996). Ice Sheet and Ice Shelf Movement detection in Test Area-Antarctica, *Proceedings of a Workshop on the Glaciological Applications of Satellite Radar Interferometry,* March 28-29, JPL.

Vachon, P.W., Geudtner, D., Mattar, K., Gray, A.L., Brugman, M., and Cumming, I. (1998). Differential SAR Interferometry Measurements of Athabasca and Saskatchewan Glacier Flow Rate, *Canadian Journal of Remote Sensing,* Vol.22, No.3, pp. 287-296.

Vaughan, D., Sievers, J., Doake, C., Hinze, H., Mantripp, D., Pozdeev, V., Sandhäger, H., Schenke, H., Solheim, A., and Thyssen, F. (1995). Subglacial and Seabed Topography, Ice Thickness and Water Column Thickness in the Vicinity of Filchner-Ronne-Schelfeis, Antarctica, *Polarforschung*, Vol. 64, No. 2, pp. 75-88.

Vaughan, D. and Doake, C.S.M. (1996). Recent Atmospheric Warming and Retreat of Ice Shelves on the Antarctic Peninsula, *Nature*, Vol. 379(letters), pp. 328-330.

Vaughan, D. and Jonas, M. (1996). Measurements of velocity of Filchner-Ronne Ice Shelf. In *Filchner-Ronne Ice Shelf Programm (FRISP),* (Report No. 10), pp. 111-116, Bremerhaven: Alfred-Wegener-Institut für Polar- und Meeresforschung.

Wexler, H. (1960). Heating and Melting of Floating Ice Shelves, *Journal of Glaciology*, Vol. 3, No. 27, pp. 626-645.

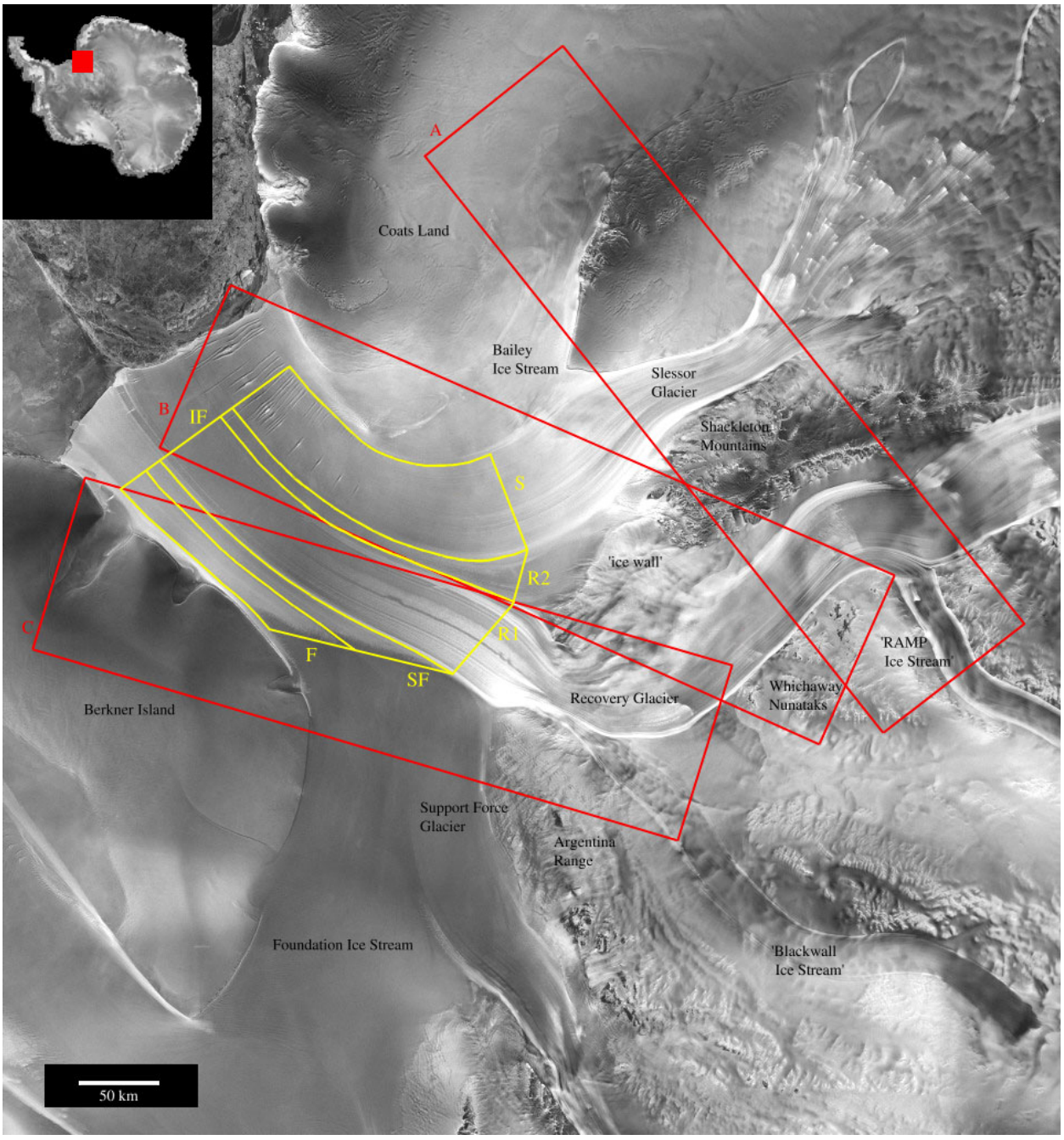

Figure 4:
Illustration, in red, of the positions of the 1997 AMM RADARSAT repeat swaths over the Filchner Ice Shelf which can be used to derive ice motion. The background image is from the AMM Antarctic mosaic and the main outlet glaciers are labelled. The yellow lines illustrate both flow lines on the Ice Shelf and the 'gates' across which the flux of ice has been estimated in Table 4. The gates are labelled: S = Slessor Glacier; SF = Support Force Glacier; F = Foundation Ice Stream; IF = Ice Front; R1 = Recovery Glacier; R2 = Recovery Glacier ice that spills over the ice fall into the ice shelf. Gates R1 and R2 are combined for the total Recovery Glacier flux.

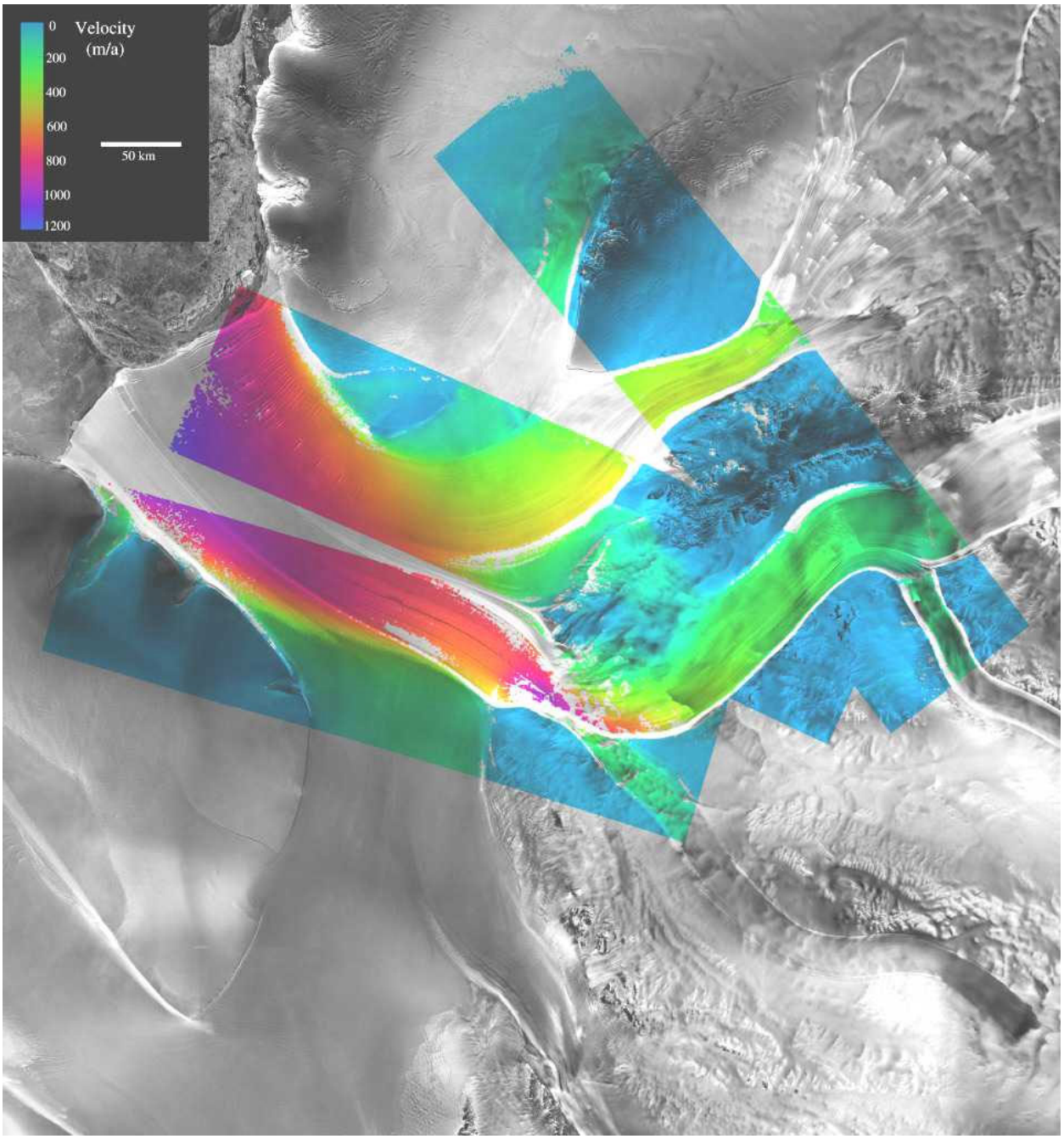

Figure 5:
Illustration of the surface velocity of the ice for the 3 swaths. Colour is used to indicate speed, as given by the inserted colour bar in the top left of the image. The low speeds are represented with blue tones, changing to red and purple for the highest speeds. The previously documented increase in speed from east to west across the front of the Filchner Ice Shelf is apparent, even with the data gap. Again, the background image is from the AMM Antarctic mosaic.

(a) Gate across Recovery Glacier

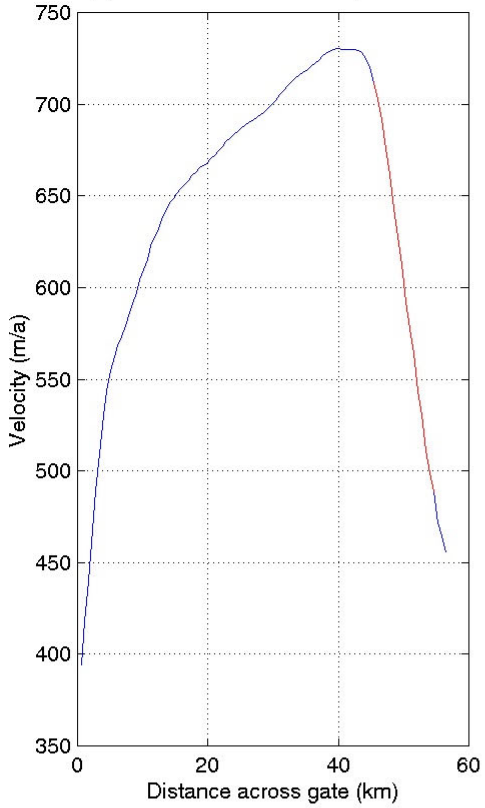

(b) Gate across Slessor Glacier

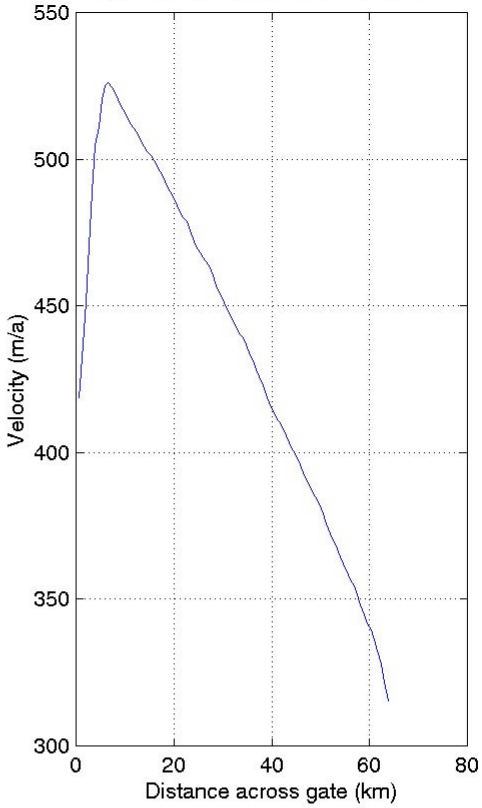

(c) Gate across ice front

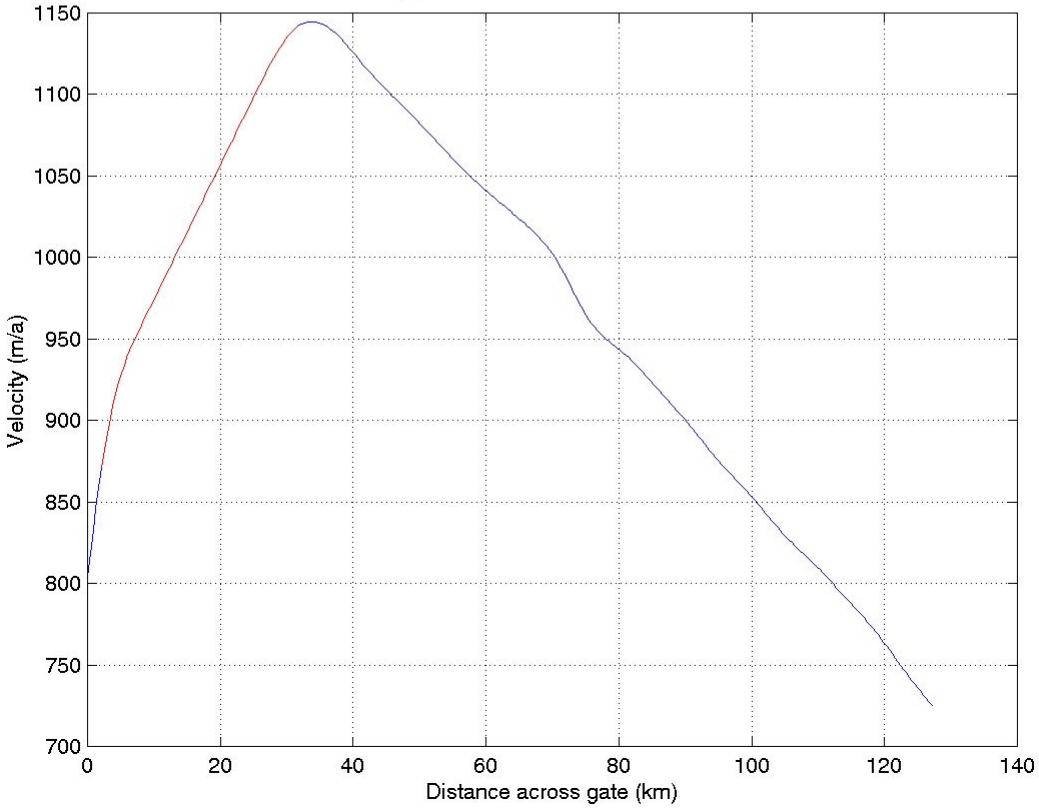

Figure 6:
Graphs showing the estimated velocity across three of the gates defined in Figure 4. The left side of the profile in (a) corresponds to the western part of gate R1, slightly downstream from the input of the Recovery Glacier. The velocity increases across the gate and peaks on the east side. The short interpolated region is necessary because of incoherence across the strong shear zone at the edge of the glacier. In (b) the velocity of the Slessor gate increases sharply to peak on the southern side of the gate and decreases almost linearly down to ~ 320 m/a on the northern (upper) side. In both (a) and (b), the estimated error is ± 21 m/a, due primarily to uncertainty in the velocity reference regions. The estimated velocity profile across the ice front gate is illustrated in (c). The velocity increases approximately linearly from the Coats Land side of the gate to peak at ~ 1145 m/a slightly on the east side of the flow stripe defining the junction of the ice from the Recovery Glacier and that from Support Force Glacier. The red region has been interpolated and uncertainties in this process contribute to the estimated ± 30 m/a error in the derived flux across this gate.